# DAMAGE SELF-SENSING BEHAVIOR OF BASALT FIBER REINFORCED POLYMER COMPOSITES MODIFIED BY ELECTROPHORETIC DEPOSITION

Dong Xiang [1] *, Haoming Sun[1], Chunxia Zhao[1], Hui Li[1], Yuanpeng Wu[1]

1 School of New Energy and Materials, Southwest Petroleum University, Chengdu 610500, China

*Corresponding author: Dr. Dong Xiang, d.xiang@swpu.edu.cn

## Abstract

In this work, basalt fiber reinforced polymer (BFRP) with enhanced electrical, mechanical properties and in-situ damage self-sensing capability was prepared using carboxylic carbon nanotubes (COOH-CNTs) modified BF fabrics via electrophoretic deposition (EPD) at different voltages. The BFRP with BF fabrics modified at a deposition voltage of 20 V (EPD20-BFRP) showed the lowest electrical resistivity. Compared with unmodified BFRP, the tensile and flexual moduli of EPD20-BFRP increased by 37.5% and 14.9%, respectively. Single-layer EPD20-BFRP exhibited a high gauge factor (GF) of 44.3 during tensile damage self-sensing. The acoustic emission (AE) signals during tensile and flexual damage process agreed well with the relative resistance changes (RRC), which confirmed different damage stages within loading process, such as elastic deformation, damage evolution, crack coalescence, and complete fracture. The multi-layer BFRP containing a single-layer EPD20-BFRP on the upper or lower surface of laminate exhibited distinct electrical signal responses subjected to the flexural loading.

## Methods

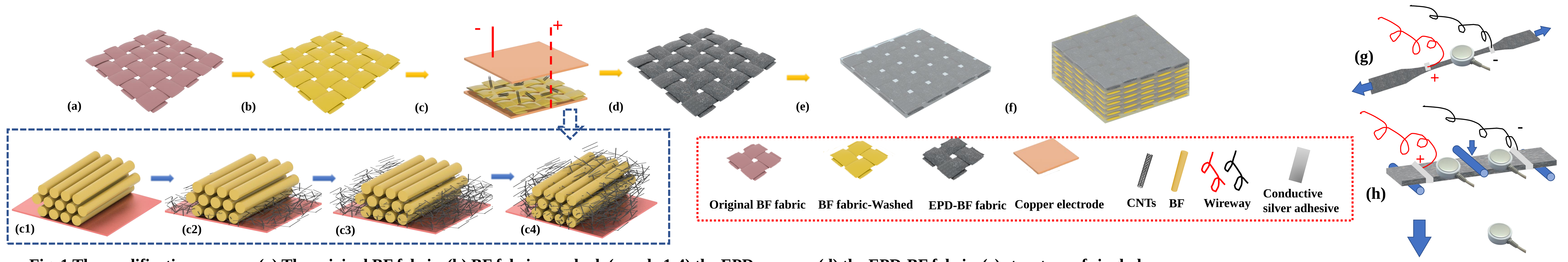


Fig. 1 The modification process: (a) The original BF fabric, (b) BF fabric -washed, (c and c1-4) the EPD process, (d) the EPD-BF fabric, (e) structure of single-layer EPD-BFRP, (f) structure of multi-layer BFRP, (g) schematic diagram of tensile specimen, (h) schematic diagram of flexure specimen.

## Morphology

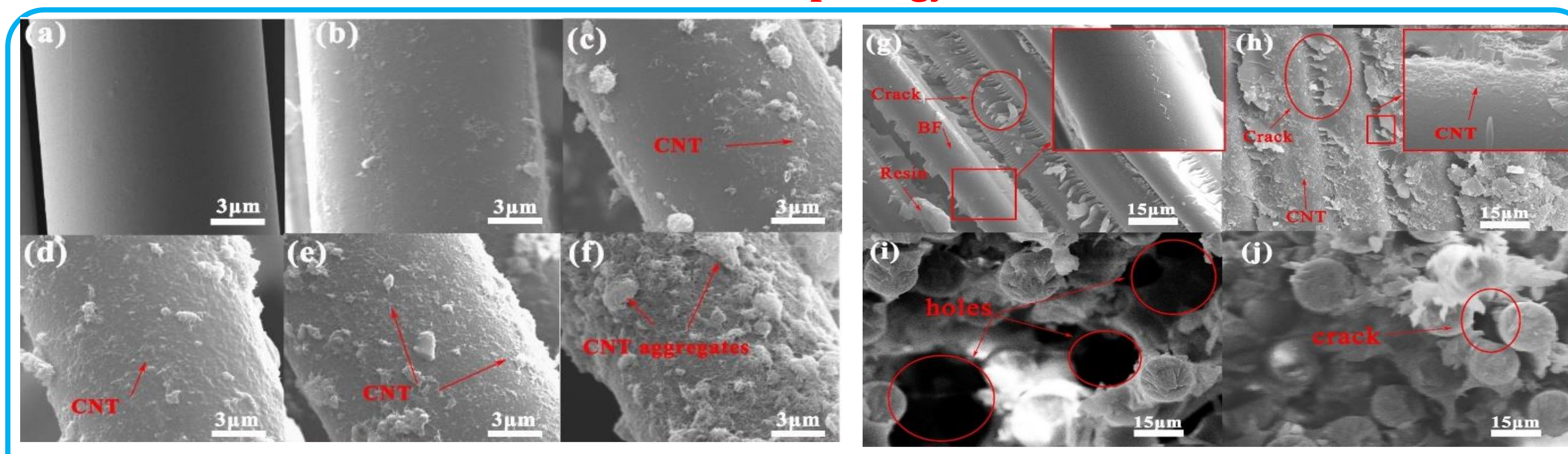


Fig. 2. SEM images showing: (a–f) The surface morphologies of the BFs subject to deposition voltages of 0, 5, 10, 15, 20, and 25 V, respectively; (g and h) BFRP and EPD20-BFRP failure surfaces, respectively; and (i and j) failure sections of BFRP and EPD20-BFRP

## Electrical properties

Table. 1 The resistivity of EPD-BFRP in different directions

| Sample | Resistivity (kΩ·mm⁻¹) In-plane | Resistivity (kΩ·mm⁻¹) Through-layer |
|---|---|---|
| BFRP | N/A | N/A |
| EPD5-BFRP | 44.2(±2.4) | 895.3(±9.4) |
| EPD10-BFRP | 39.1(±3.1) | 600.4(±7.0) |
| EPD15-BFRP | 36.8(±2.1) | 313.78(±3.8) |
| EPD20-BFRP | 34.8(±1.6) | 233.4(±7.1) |
| EPD25-BFRP | 35.1(±3.3) | 247.6(±1.3) |

Table. 2 Change ratio of the EPD-BFRPs mechanical properties at different EPD deposition voltages

| Sample | $\Delta E_t$ (%) | $\Delta\sigma_t$ (%) | $\Delta\varepsilon_t$ (%) | $\Delta E_f$ (%) | $\Delta\sigma_f$ (%) | $\Delta\varepsilon_f$ (%) |
|---|---|---|---|---|---|---|
| EPD 5-BFRP | + 9.9 | + 6.6 | + 2.0 | + 3.5 | + 6.9 | + 4.5 |
| EPD10-BFRP | + 13.2 | + 7.8 | + 6.4 | + 6.7 | + 15.0 | + 9.6 |
| EPD15-BFRP | + 23.8 | + 13.7 | + 8.4 | + 11.3 | + 19.4 | + 13.8 |
| EPD20-BFRP | + 37.5 | + 23.6 | + 13.7 | + 14.9 | + 28.3 | + 21.7 |
| EPD25-BFRP | + 27.4 | + 22.2 | + 14.5 | + 12.2 | + 23.1 | + 19.6 |

## Mechanical properties

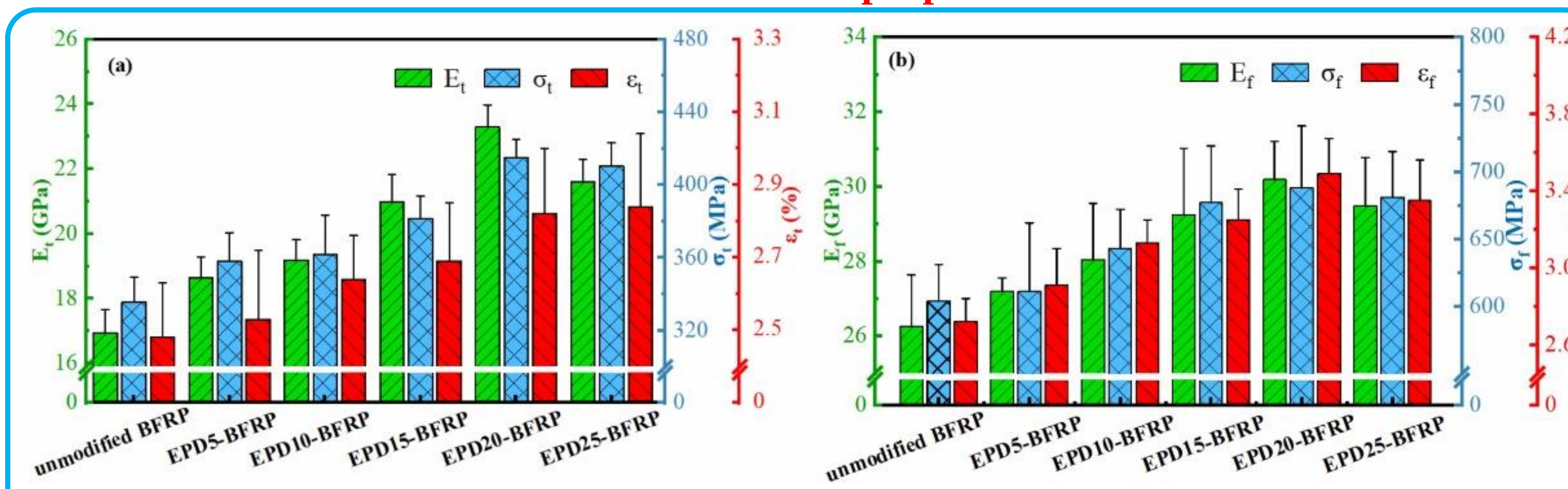


Fig. 3 Mechanical properties of the BFRPs produced at different EPD deposition voltages: (a) tensile property and (b) flexural property.

## Damage self-sensing properties

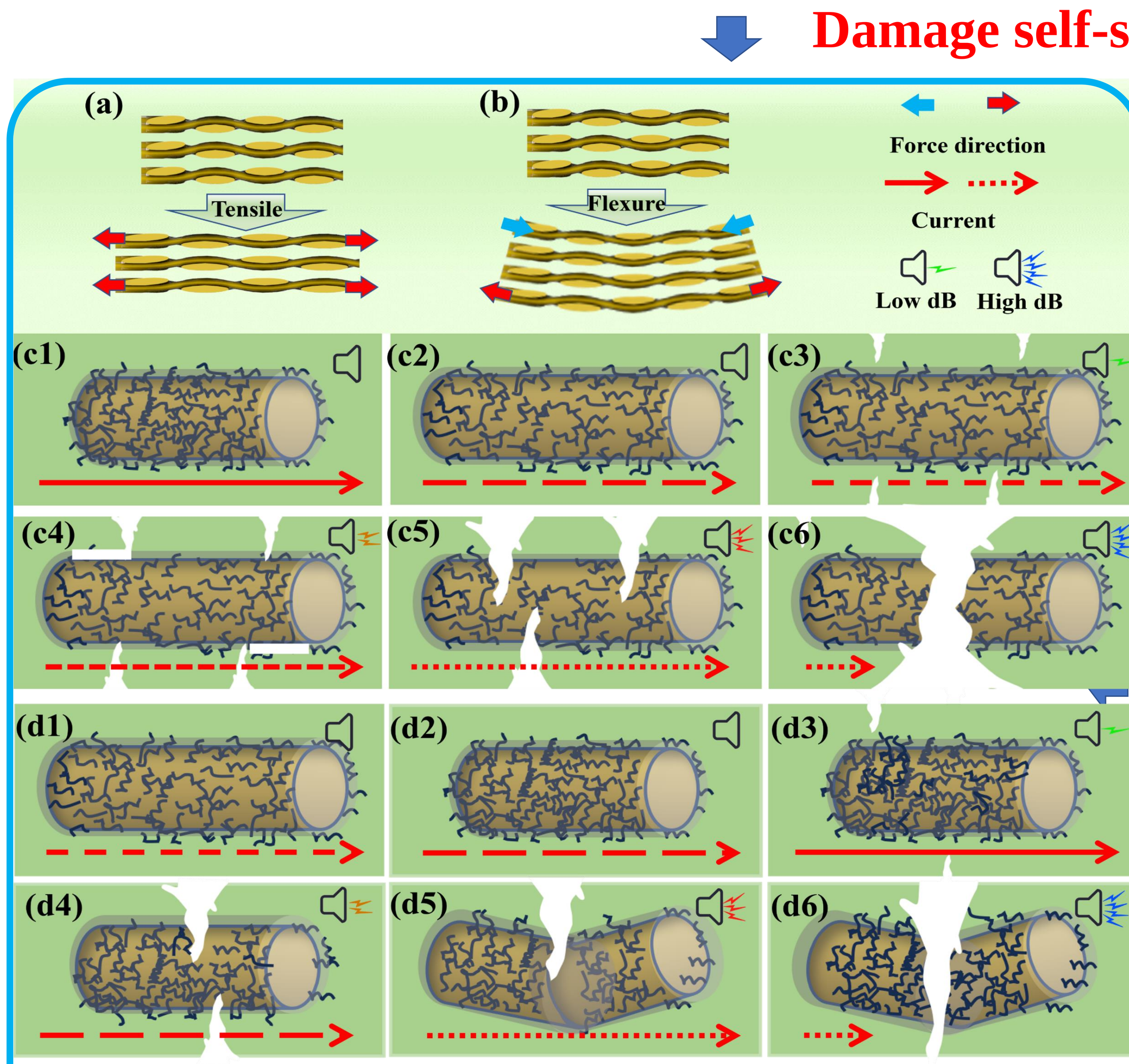


Fig.4 Schematic diagrams of the damage and electrical property evolution of EPD-BFRP. (a) tensile load applied, (b) flexural load applied, (c1-c6) tensile failure process and (d1-d6) flexural failure process.

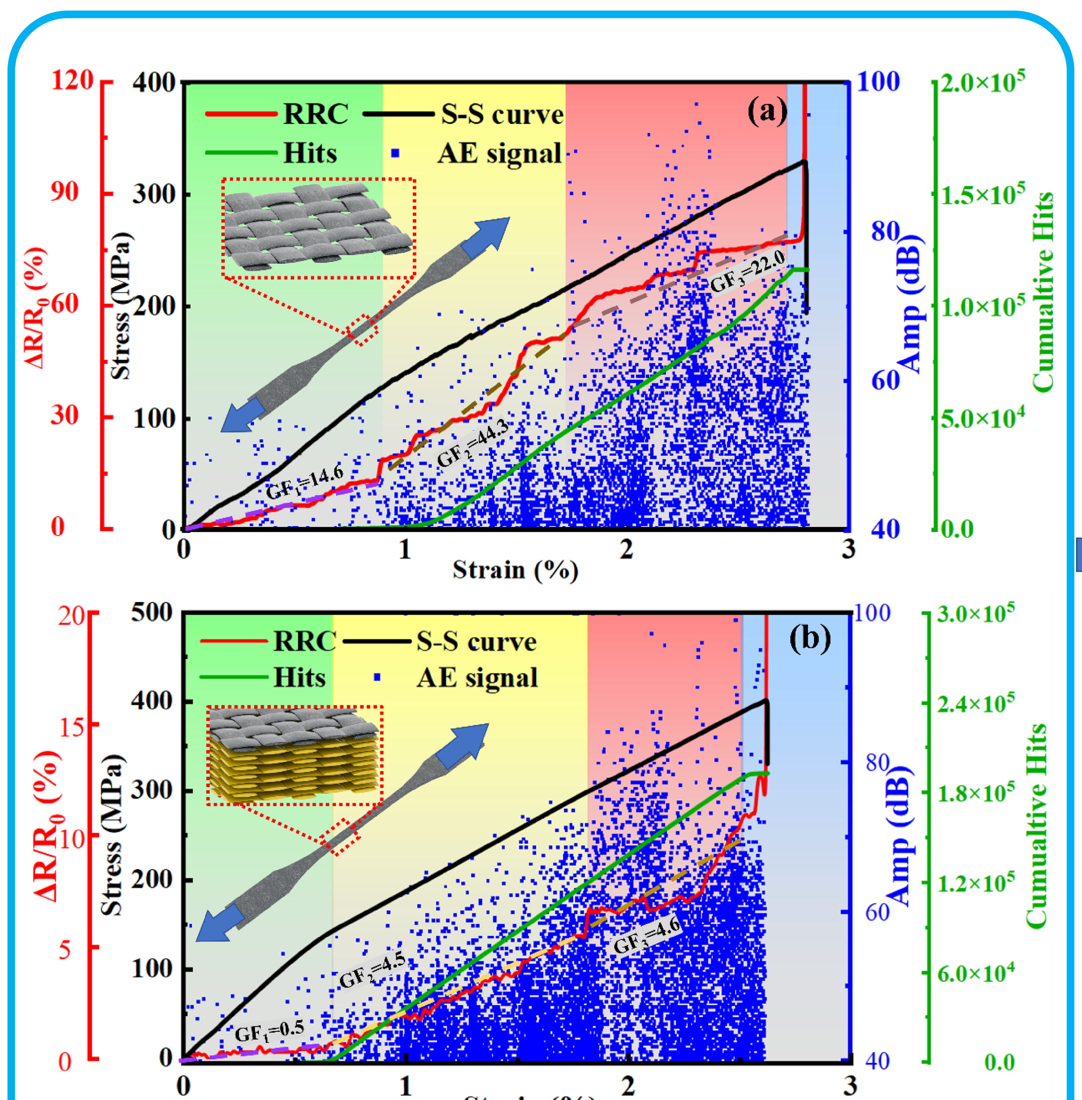


Fig. 5 RRC, Stress-strain, and AE signals during tensile process. (a) single-layer BFRP, (b) mulitlayer BFRP .

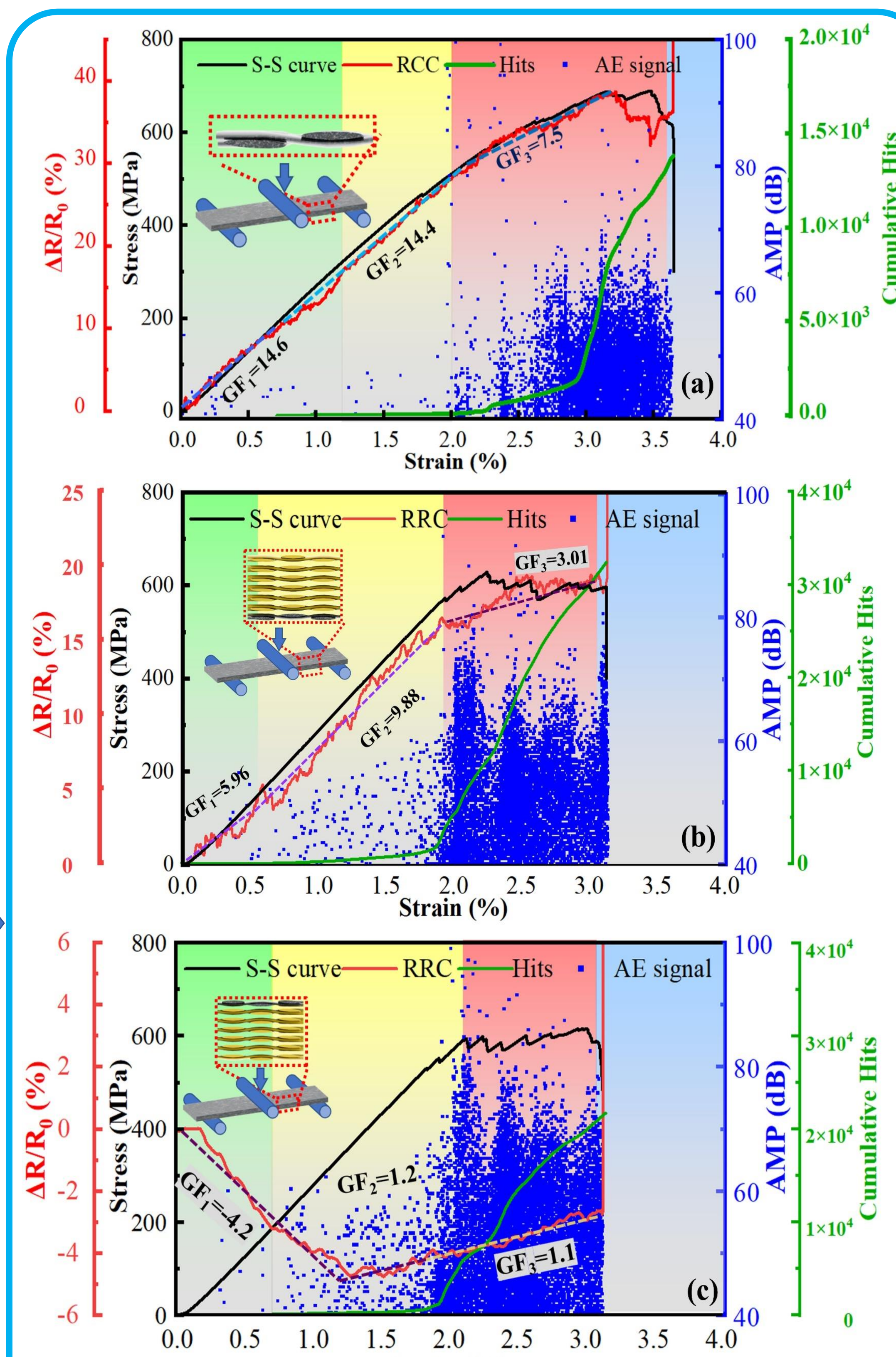


Fig.6 RRC, Stress-strain curve, and AE signals during flexual. (a) single-layer BFRP, (b) multi-layer BFRP with a functional layer at the bottom and (c) multi-layer BFRP with a functional layer at top.

## Conclusions

A BFRP with damage self-sensing property was prepared by electrical deposition of CNT. Single-layer EPD20-BFRP exhibited a high gauge factor (GF) of 44.3 during tension and 14.6 during flexure. For the functional layer at lower surface, the RRC increased lineary in elastic deformation and damage evolution stages. The multi-layer BFRP containing single-layer EPD20-BFRP exhibited distinct RRC responses subjected to the flexural loading on the upper or lower surface. This behavior can be used to identify the direction of stress applied to the structure. The results obtained in this work indicate that EPD-BFRP is suitable for in-situ damage detection of BF reinforced composite materials.

## Acknowledgement

• This work was supported by the National Natural Science Foundation of China (12102374, 52173301); Sichuan Science and Technology Program (2021YFH0031, 2022JDGD0015, 2022YFH0019, 2022YFG0113)